

1 ***Wilms Tumor 1b* defines a wound-specific sheath cell**
2 **subpopulation associated with notochord repair**

3 Juan Carlos Lopez-Baez^{1,2}, Zhiqiang Zeng^{1,2}, Witold Rybski^{1,2}, Leonie F.A. Huitema³,
4 Alessandro Brombin^{1,2}, Rodney M. Dale⁴, Koichi Kawakami⁵, Christoph Englert⁶,
5 Stefan Schulte-Merker^{3,7}, Nicholas D. Hastie^{1*}, E. Elizabeth Patton^{1,2*}

6

7 1. MRC Human Genetics Unit, MRC Institute for Genetics and Molecular Medicine,
8 University of Edinburgh, Crewe Road, Edinburgh, EH4 2XR.

9 2. CRUK Edinburgh Centre, MRC Institute for Genetics and Molecular Medicine, University
10 of Edinburgh, Crewe Road, Edinburgh, EH4 2XR.

11 3. Hubrecht Institute – KNAW & UMC Utrecht, Uppsalalaan 8, 3584CT Utrecht, NL

12 4. Department of Biology, Loyola University Chicago Quinlan 222 1032 W. Sheridan Road,
13 Chicago, IL 60660 USA

14 5. Division of Molecular and Developmental Biology, National Institute of Genetics 1111
15 Yata, Mishima Shizuoka, 411-8540 Japan

16 6. Department of Molecular Genetics, Leibniz Institute for Age Research-Fritz Lipmann
17 Institute (FLI), Beutenbergstrasse 11, Jena, Germany, and Institute of Biochemistry and
18 Biophysics, Friedrich-Schiller-University Jena, 07745 Jena, Germany

19 7. Institute for Cardiovascular Organogenesis and Regeneration, Westfälische Wilhelms-
20 Universität, Mendelstraße 7, 48149 Münster

21

22 *Correspondence to: nick.hastie@igmm.ed.ac.uk; e.patton@igmm.ed.ac.uk

23

24 **Impact statement**

25 Wound-specific notochord sheath cell subpopulations associate with notochord repair and
26 adult vertebrae formation.

27

28

29 **Abstract**

30 Regenerative therapy for degenerative spine disorders requires the identification of cells that
31 can slow down and possibly reverse degenerative processes. Here, we identify a novel and
32 unanticipated wound-specific notochord sheath cell subpopulation that expresses Wilms
33 Tumor (WT) 1b following injury. Using live imaging in zebrafish, we show that localized
34 damage leads to *Wt1b* expression in the sheath, and that *wt1b+* cells migrate into the wound
35 to form a stopper-like structure, likely to maintain structural integrity. At the wound *wt1b+* and
36 *entpd5+* cells constitute distinct subpopulations, and mark the site of an extra vertebra that
37 forms in an untypical manner via a cartilage intermediate. Surprisingly, *wt1b+* cells become
38 closely associated with the chordacentra and sustain *wt1b* expression for over 35 days during
39 vertebra formation. Given that remnants of notochord cells remain in the adult intervertebral
40 disc, the identification of novel subpopulations may have important implications for
41 regenerative treatments for spine disorders.

42

43 **Highlights**

- 44 • Notochord injury triggers wound-specific expression of *wt1b* in novel sheath subpopulation
- 45 • WT1b notochord sheath cells fill injury site and form stopper-like structure
- 46 • WT1b subpopulation marks site of a new vertebra that forms via a cartilage intermediate
- 47 • WT1b wound-specific subpopulation perdures throughout and after vertebra repair

48

49 **Introduction**

50 Wilms' tumour 1 (WT1) is a zinc finger transcription factor that regulates key developmental
51 stages of several mesodermal tissues including the kidneys, gonads and coronary
52 vasculature (Hastie 2017). In the developing kidney, WT1 is required for the maintenance of
53 mesenchymal nephron progenitors (Kriedberg et al, 1993, Motamedi et al, 2014) as well as
54 differentiation of these progenitors into the epithelial components of the nephron (Essafi et al,
55 2011). In contrast, in the developing heart, WT1 is expressed in the epicardium (mesothelial
56 lining) and required for the production, via an epithelial to mesenchymal transition (EMT), of
57 coronary vascular progenitors (EPDCs) that migrate into the myocardium (Martinez-Estrada
58 et al., 2010). Similarly, WT1-expressing mesothelium is the source of mesenchymal
59 progenitors for specialised cell types within several other developing organs. These include
60 stellate cells within the liver (Asahina et al, 2008), interstitial cells of Cajal in the intestine
61 (Carmona et al, 2013) and adipocytes within visceral fat depots (Chau et al, 2014). WT1
62 expression is down-regulated in the epicardium postnatally but reactivated in response to
63 tissue damage in both mice (Smart et al., 2011) and zebrafish (Schnabel et al., 2011). In both
64 organisms, this activation of WT1 in response to damage is associated with new rounds of
65 epicardial EMT, leading to the production of coronary vascular progenitors (Smart et al.,
66 2011; Schnabel et al., 2011).

67 Given the reactivation of *Wt1/wt1b* in the damaged epicardium we set out to investigate
68 whether WT1 programmes are initiated in response to other sources of tissue damage in
69 zebrafish, and uncovered a novel *Wt1* response to wounding of the notochord. The notochord
70 is a transient embryonic structure that provides axial support, signalling information, and is
71 required for vertebrae development and formation (Stemple et al., 2005). The notochord is
72 comprised of two cell populations, the inner vacuolated cells that provide rigid support to the
73 embryo, and the outer sheath cells, a single cell epithelial layer that surrounds the vacuolated
74 cells and secretes components of the extracellular matrix to provide turgor pressure to the
75 vacuolated cells (Ellis *et al.*, 2013; Apschner et al., 2011). This rigid axial structure eventually
76 is replaced by vertebrae bone. In zebrafish, a row of metameric mineralized rings, known as
77 chordacentra, forms around the notochord in an anterior to posterior fashion and constitute
78 the first signs of the definitive vertebrae. The chordacentra delineate the future sites where

79 mature vertebra will form and ossify as the larva grows, while the notochord cells develop into
80 the nucleus pulposus of the adult intervertebral disk, a soft gel-like tissue that provides
81 cushioning and flexibility for the spine.

82 Degeneration of the intervertebral disk leads to extensive back pain, one of the top global
83 causes of years lived with disability (Lawson & Harfe, 2015). Treatment primarily consists of
84 managing the pain symptoms, or in more progressed disease includes extensive surgery.
85 One of the major goals of the tissue-engineering field is to identify cells and tissues that will
86 enable novel regenerative therapies to slow down and possibly reverse the degenerative
87 process. Here, we uncover a novel cellular subpopulation in the notochord sheath that
88 emerges at the site of damage and is maintained until formation of a repaired adult vertebra
89 structure. Surprisingly, this subpopulation expresses *wt1b* despite no evidence of *wt1b*
90 expression in physiological notochord development or ossification. Our findings suggest that
91 the zebrafish notochord is protected by a novel wound-specific programme that seals the
92 notochord wound in the embryo and establishes the site of a new adult vertebra.

93 **Results**

94 **Wound specific expression of *wt1b* in the notochord**

95 Given the expression of *wt1b* in the regenerating heart, we wanted to explore the expression
96 of *wt1* in other regenerating tissues, and began with the tail fin regenerative processes. There
97 are two *wt1* paralogues in zebrafish, *wt1a* and *wt1b*, and so we performed tail fin amputations
98 on zebrafish larvae 3 days post fertilization (dpf) using *Tg(wt1a:GFP)* and *Tg(wt1b:GFP)*
99 transgenic lines (Bollig *et al.*, 2006; Perner *et al.*, 2007; **Supplementary Figure 1a**).
100 Surprisingly, we discovered that tail fin amputations that included partial removal of the
101 notochord triggered a change of cellularity in the notochord, coupled with the specific, *de*
102 *novo* upregulation of GFP in a *Tg(wt1b:GFP)* transgenic line. This response was specific to
103 *wt1b* because we did not observe expression of GFP in *Tg(wt1a:GFP)* tail fin amputated
104 larvae (**Supplementary 1b-e**).

105
106 Next, we developed a needle-based assay to specifically induce localized damage in the
107 developing zebrafish notochord independent of tail fin amputation. Needle injury was induced
108 in 3 dpf *Tg(wt1b:GFP)* that had been crossed with *casper* fish to remove pigmentation and

109 imaged at 72 hours post injury (hpi) (**Figure 1a**). Needle induced wounds triggered a similar,
110 albeit stronger *wt1b:GFP* response to the tail fin amputations, that was specifically localised
111 to the site of the wound (**Figure 1b**). Time course imaging showed a progressive expansion
112 of the damaged area over 72 hours, with an increasing expression of GFP signal,
113 concomitant with a change of cellularity in the notochord (**Figure 1c**). Importantly, this was
114 not observed in uninjured zebrafish controls (**Figure 1c**) or in notochord injured
115 *Tg(wt1a:GFP)* transgenic larvae (data not shown). Histological staining of the damaged area
116 revealed the presence of a subpopulation of cells at the site of injury, which contrasted
117 morphologically with the uniform, vacuolated inner cells of the notochord (**Figure 1d**). These
118 cells stained positively for GFP and for endogenous Wt1 protein by immunohistochemistry,
119 validating the faithful expression of the transgene with endogenous *wt1b* expression in this
120 response (**Figure 1e**). Thus, following notochord injury, an unanticipated expression of *wt1b*
121 marks a subpopulation of cells that emerges in the notochord and is associated with the
122 wound.

123 ***wt1b* expressing cells emerge from the notochord sheath**

124 To determine the origin of the wound-specific *wt1b*⁺ cells, we examined *wt1b* expression in
125 the notochord and vacuolated cells, using a *Tg(SAGFF218:GFP)* transgenic line that labels
126 the membrane of the inner vacuolated cells and *Tg(col2a1a:RFP)* that is specifically
127 expressed in the surrounding notochord sheath cells (**Figure 2a**; Yamamoto *et al.*, 2010 and
128 Dale and Topczewski, 2011).

129 A needle-induced notochord wound in the *Tg(SAGFF214:GFP)* transgenic line showed that
130 GFP-expressing cells were lost rapidly upon injury, creating a gap in the row of vacuolated
131 cells. Eventually, this gap was filled with new cells by 144 hpi (**Supplementary Figure 2a,b**).
132 The *SAGFF214:GFP* response was distinct from the *wt1b*⁺ response in time (emerging at 72
133 hpi compared with 24 hpi), size and number (few and large compared with numerous and
134 small), and in coverage of the wound (visible gaps remaining at the site compared with filling
135 the damage site). These data suggest that *wt1b* expressing cells are distinct from the
136 vacuolated cells at the site of injury.

137 Next, we explored the role of the notochord sheath cells in this process. We crossed the
138 *Tg(wt1b:GFP)* transgenic line to a *Tg(col2a1a:RFP)* transgenic line, generated with a 1 KB
139 fragment of the *col2a1a* promoter that is transiently expressed in the sheath cells until
140 approximately 6 dpf (Dale & Topczewski, 2011). Live confocal and multiphoton imaging
141 revealed *wt1b:GFP* expression in the *col2a1a:RFP* notochord sheath cells following needle
142 induced notochord damage (**Figure 2 b-d**; **Video 1**; **Supplementary Figure 2c,d**).
143 *Wt1b:GFP* co-expression with *col2a1a:RFP* was visible by 24 hpi in a ring surrounding the
144 notochord vacuolated cells, and by 72 hpi the *wt1b:GFP* subpopulation of sheath cells had
145 migrated into the inner lumen of the notochord to fill the wound and produce a visible stopper-
146 like seal in the notochord.

147 To validate the co-expression of *wt1b:GFP* and *col2a1a:RFP* in the wounded fish, we FACS
148 sorted cell populations in the injured versus uninjured larvae isolated from the trunk region
149 (**Figure 2e**; n = 35 larvae per set). While GFP+ only and RFP+ only expressing cells were
150 found in both injured and non-injured larvae, only the wounded fish had cells that co-
151 expressed *wt1b:GFP* and *col2a1a:RFP* (GFP+RFP+; 289 cells vs. 3 cells respectively).

152 Our evidence indicates that the notochord wound triggers a unique *wt1b+* subpopulation to
153 emerge in the notochord sheath cells. This *wt1b+* sheath cell subpopulation migrates into the
154 wound and generates a stopper-like structure, possibly to prevent further loss of notochord
155 turgor pressure and maintain notochord integrity.

156 **Notochord wounds express cartilage and mesenchyme genes**

157 To address the molecular process at the site of the wound, we compared the transcriptome of
158 the trunk region in the injured and uninjured 72 hpi larvae (**Figure 3a, b**; n = 50 larvae per
159 subset). Microarray analysis revealed a highly significant 131-fold increase in expression of
160 *matrix gla protein (mgp)*, a gene that is known to express in chondrocytic zebrafish tissues
161 (Gavaia *et al.*, 2006) and to be involved in the inhibition of hydroxyapatite production during
162 ectopic bone formation (Zebboudj *et al.*, 2002; Sweatt *et al.*, 2003; Schurgers *et al.*, 2013)
163 (**Figure 3c, d**). Other genes included mesenchymal and cell adhesion markers, such as *fn1b*,
164 coagulation factors, such as *f13a1b*, and immune response genes, such as *zgc:92041* and
165 complement c6 (**Figure 3d**).

166 The increased expression of *mgp* and *f13a1b* genes implicated the *de novo* acquisition of
167 chondrogenic features in the injured tissues. Chondrogenic cells in the endochondral tissues
168 of the craniofacial, fin bud and axial skeletons express *mgp* (Gavaia *et al.*, 2006) and *FXIIIa*
169 expression is localized to the developing chondrogenic mesenchyme of the pectoral fin bud
170 (Deasey *et al.*, 2012). The expression of cartilage genes was unexpected because
171 ossification of the zebrafish notochord occurs via the formation the chordacentra, and does
172 not require the establishment of cartilage anlagen (Flemming 2004; Bensimon-Briti *et al.*,
173 2012; Lefebve & Bhattaram, 2010). To examine the expression of other chondrogenic genes,
174 we analyzed the top 100 significant genes and found an increase in expression in Sox9, the
175 master regulator of chondrogenesis, five collagen genes associated with chondrogenic
176 tissues (*col2a1a*, *col2a1b*, *col11a2*, *col9a1* and *col9a2*), the cartilage specific extracellular
177 structural protein Aggrecan, a microRNA regulator of chondrogenesis microRNA140 and the
178 matrix-cell anchor protein chondroadherin (*chad*) (**Figure 3e**). Our results reveal that
179 notochord wounding leads to an unexpected increase in expression of genes associated with
180 cartilage.

181 **Extra vertebra forms at the repair site via an unusual cartilage intermediate**

182 The expression of cartilage genes suggests that the notochord wound may induce a
183 previously unknown and alternative bone development process. We stained injured and
184 control animals with alcian blue and alizarin red stains, which highlight the cartilage and bone
185 respectively. Cartilage was clearly visible at the site of injury as soon as 3 dpi. This staining
186 was significantly stronger and distinct from the highly coordinated segmental cartilage
187 staining that normally occurs during zebrafish vertebra development, which is clearly visible in
188 both injured and non-injured controls by 14 dpi (**Figure 4a**). Similarly, the alizarin red dye
189 identified the anterior to posterior forming chordacentra rings during larval development.
190 However, in injured zebrafish larvae, the normally uniform mineralization pattern was
191 interrupted around the site of damage, leading to delayed formation of the chordacentra at
192 later stages (**Figure 4a**).

193 By 18 dpi, the injured site began to express bone matrix, and was visibly flanked by cartilage
194 expressing segments (**Figure 4b**). This was unusual because in development of the
195 vertebrae, cartilage and bone stains mark distinct regions of the notochord. To evaluate the

196 outcome of the injury in the bone process, wild-type larvae were injured and stained in calcein
197 dye at 21 and 38 dpi (Du *et al.*, 2001). Interestingly, the needle injury led to a delayed
198 vertebral formation at the site of damage. These vertebrae that eventually formed were
199 smaller and supernumerary, such that injured fish had one more vertebrae than their
200 uninjured age-matched controls (**Figure 4 c-e**).

201 The notochord provides signals for the patterning of vertebral and spine formation via the
202 patterned activation of various signals, and has been proposed to be an essential component
203 of chordacentra formation (Flemming *et al.*, 2004; Bensimon-Brito *et al.*, 2012). The
204 *Tg(entdp5:RFP)* transgenic line marks osteoblastic cells responsible for the patterned
205 formation of chordacentra rings, and serves as a readout for mineralizing activity (Huitema *et*
206 *al.*, 2012). *Entpd5* (ectonucleoside triphosphate diphosphohydrolase 5) is an E-type NTPase
207 that is found in bone mineralizing environments and is essential for skeletal morphogenesis
208 (Huitema *et al.*, 2012). We crossed the *Tg(wt1b:GFP)* transgenic line to *Tg(entdp5:RFP)* and
209 followed the wound response. *wt1b* and *entpd5* expressing cells populations were closely
210 associated at the wound site indicating that mineralizing *entpd5* cells may directly contribute
211 to *wt1b+* associated chordacentra (**Figure 5 a,b**).

212 **Embryonic *wt1b+* subpopulations perdure into the adult vertebrae**

213 We noticed that the *Tg(wt1b:GFP)* transgene expression was always associated with the site
214 of new vertebrae formation in the injured zebrafish that were raised to adulthood. To
215 determine if *wt1b* expression was transient at the wound, or sustained throughout the repair
216 process, we raised needle injured *Tg(wt1b:GFP; casper)* zebrafish larvae for up to 38 days
217 (**Figure 6a**).

218 GFP expression was sustained at the wound site, remaining in a small, cellular population at
219 the site of damage, even as chordacentra developed and mineralized around the notochord
220 over time (**Figure 6a, b, c**). Small GFP expressing cells were further confirmed by α -GFP
221 staining at the site of damage (**Figure 6b**) Strikingly, the *Tg(wt1b:GFP)* transgene maintained
222 expression at this site up to 38 dpi (**Figure 6d**) before eventually reducing expression.

223 To gain a better understanding of how *wt1b:GFP* expressing cells engage with the newly
224 forming vertebrae, we carried out confocal imaging of the area of damage. The analysis

225 revealed the presence of both fused and unfused vertebrae at the damaged site, and the
226 sustained and strong expression of *wt1b:GFP* expressing cells associated with the
227 developing ectopic vertebra at the repair site area (**Figure 6e,f**).

228 Taken together these results indicate that *wt1b:GFP* expressing cells both mark a
229 subpopulation of cells that are rapidly activated at the site of the wound and also that these
230 cells persist until adulthood, possibly orchestrating local vertebrae formation.

231

232 **Discussion**

233 Our analysis has uncovered wound-specific cellular heterogeneity in the zebrafish notochord
234 that perdures during adult vertebra formation at the injury site (**Figure 7**).

235 Despite *wt1b* having no reported role in notochord development, and despite not being
236 expressed in the notochord, we identified a specific *de novo* expression of *wt1b* following
237 notochord wounding. The activation of *wt1b* in sheath cells that migrate into the notochord is
238 reminiscent of the situation where *wt1b* expression is reactivated in epicardial cells that
239 undergo EMT to produce vascular progenitors and migrate into the heart (Martinez-Estrada et
240 al., 2010). This raises the question whether notochord sheath cells may also be mesothelial in
241 nature and if the invading *wt1b* expressing cells are produced via an EMT or, perhaps more
242 accurately, a mesothelial to mesenchyme transition.

243 Wounding leads to localized *wt1b* expression in the notochord sheath cells that invade the
244 site of the injury to form a stopper-like structure, likely to maintain notochord integrity. Very
245 recently, Bagnet and colleagues reported the identification of notochord sheath cells involved
246 in the replacement of vacuolated cells lost due to motion-dependent mechanical damage to
247 the notochord (Garcia et al., 2017). In this context, sheath cells invade the vacuolated cell
248 layer and differentiate into vacuolated cells to maintain turgor pressure. In light of this report,
249 we have reanalysed our image analysis, but find no evidence to support that *wt1b* cells
250 become vacuolated cells following acute wounding. In contrast, we find *wt1b*-expressing cells
251 tightly associated with a stopper-like (scar-like) structure and continued *wt1b* expression at
252 the wound site even during formation of an ectopic vertebra. We also detected *entpd5*
253 expressing cell subpopulations at the wound that are distinct from *wt1b* expressing cells.
254 These studies highlight a previously unknown complex and heterogeneous nature of the

255 sheath, and suggest that the notochord sheath can sense and respond to different types of
256 damage. Motion-dependent shear stress causes loss of vacuolated cells that are replaced by
257 new vacuolated cells that arise from the sheath (Garcia et al., 2017), while acute damage (i.e.
258 needle injury) that encompasses sheath and vacuolated cell damage, leads to sheath cells
259 forming a seal that marks the site of new cartilage and vertebra (**Figure 7**).

260 By leveraging gene expression profiling of the wounded tissue, we discovered an alternative
261 mechanism for vertebra formation via a cartilage intermediate at the injury site. This was
262 unexpected because in zebrafish, ossification of chordacentra does not require the
263 establishment of cartilage anlagen, but rather arises from the osteoblastic maturation of
264 mesenchymal cells at the site of bone formation (Lefebvre & Bhattaram, 2010). Our
265 observations indicate a wound-specific response to vertebra development. Vertebrae at the
266 wound are supernumerary and smaller, with some showing defective neural and hemal
267 arches (data not shown), and continue to be closely associated with *wt1b*+ cells until fully
268 formed. We noted that the kinetics of vertebra formation at the damage site was delayed
269 compared with other vertebrae. This delay could be explained by the very high expression of
270 the cartilage gene *mgp* that inhibits calcification and BMP2 in mineralizing tissues (Schurgers
271 et al., 2013; Zebboudj et al., 2002; Sweatt et al., 2003). This alternative mode for vertebra
272 formation at the wound site may be a salvage structure to effectively maintain structural
273 integrity of the developing axial skeleton.

274

275 **Materials and Methods**

276 All experimental procedures were approved by the University of Edinburgh Ethics Committee
277 and were in accordance with the UK Animals (Scientific Procedures) Act 1986.

278 **Zebrafish lines**

279 Transgenic lines for this study include: *Tg(entpd5:RFP)* (Huitema et al., 2012), *Tg(ubi:switch)*
280 (Mosimann et al., 2011), *Tg(SAGFF214:GFP)* (Yamamoto et al., 2010), *Tg(wt1a:GFP)* (Bollig
281 et al., 2009), *Tg(wt1b:GFP)* (Perner et al., 2007; Bollig et al., 2009). Many of the studies were
282 performed in a transparent background created by crossing homozygous *Tg(wt1b:GFP)* fish
283 to homozygous pigment-free transparent *casper* fish (White et al., 2008). The

284 *Tg(wt1b:GFP;col2a1a:RFP)* line was created by injecting the R2-*col2a1a:mCherry* construct
285 (Dale and Topczewski, 2011) with a Tol2 transposase (Kawakami, 2007) into
286 *Tg(wt1b:GFP;casper)* zebrafish embryos.

287 **Notochord needle injury and tail amputation assays**

288 Larvae were anaesthetised in tricaine, placed sagittally on a petri dish and either inserted
289 gently with an electrolysis-sharpened tungsten wire or tail amputated at different levels.
290 Injured larvae were transferred to fresh water to recover and observe. Non-injured age-
291 matched larvae were grown as non-injured controls.

292 **Whole-mount microscopy**

293 Live and fixed whole-mount time-course and time-lapse experiments were performed using
294 an AZ100 upright microscope (Nikon) using a x2 and x5 lens with a Retiga Exi camera
295 (Qimaging) or Coolsnap HQ2 camera (Photometrics). Images were analyzed and processed
296 using the IPLab Spectrum and Micro-Manager softwares. Live and fixed whole-mount
297 confocal imaging was performed using an A1R confocal system (Nikon) using a x20 lens over
298 a Z-plane range of 80-100 μm (approximate width of the notochord) using a 480nm laser
299 (GFP) and/or a 520nm laser (RFP) lasers. Images were captured and analysed using Nis-
300 Elements C software (Nikon). Multiphoton confocal time-lapse imaging was performed using
301 an SP5 confocal microscope (Leica) equipped with a Ti:Sapphire multiphoton laser (Spectra
302 Physics) and a 3 axis motorised stage. For confocal imaging and time-lapse experiments,
303 anaesthetised injured and non-injured larvae were embedded sagittally in a drop of 1% low-
304 melting point agarose prior to imaging, in a specially designed glass insert, which was
305 covered in a mixture of E3 medium and anaesthetic. All time-lapse imaging was done at 30 or
306 60 mins intervals over 48 hours using an incubation chamber (Solent Scientific) under a
307 constant temperature of 28°C and larvae were terminated in an overdose of tricaine at the
308 end of each the experiment.

309 **Histology**

310 Zebrafish larvae younger than 20 dpf were culled and fixed overnight in 4% PFA/PBS at 4°C.
311 The fixed larvae were washed in PBS, dehydrated in rising methanol/PBS concentrations and
312 cleared in xylene before being paraffin embedded for sectioning. Older zebrafish were culled
313 and fixed in 4% PFA/PBS at 4°C for 3 days with an abdominal incision to ensure tissue

314 penetrance of the fixative (Wojciechowska et al., 2016). Fish were decalcified using 0.5M
315 EDTA (pH 7.5) for 5 days in a rocker at 4°C and dehydrated in 70% ethanol at 4°C. Fish were
316 embedded in paraffin using a Miles Scientific Tissue TEK VIP automated processor.
317 Embedded larvae and older zebrafish were sectioned using a Leica RM2235 rotary
318 microtome to a width of 5 µm. Sections were haematoxylin and eosin (H&E) stained and
319 mounted using DPX mounting media (Sigma-Aldrich). For cryosections, zebrafish larvae were
320 embedded in OCT (Tissue Tek) and cut to 8 µm following protocols available at www.zfin.org.

321 **Immunohistochemistry**

322 Slides were de-waxed in xylene and rehydrated through decreasing ethanol washes, before
323 being incubated in a bleach solution to remove pigment. Antigen-unmasking was performed
324 as previously described (Patton *et al.*, 2005). The slides were DAB stained following
325 manufacturer's instructions (Dako). Slides were incubated overnight at 4°C with the following
326 antibodies: α -GFP (1:1,500; Cell Signaling Technology) and α -WT1 (1:25,000). The α -WT1
327 was designed using the TARGET antibody production protocol from Cambridge Research
328 Biochemicals using a conserved protein sequence from the C-terminal of the zebrafish Wt1a
329 and Wt1b proteins. An Axioplan II fluorescence microscope (Zeiss) with a Plan Aplanachromat
330 objective was used for brightfield imaging of tissue sections. Images were captured using a
331 Qimaging Micropublisher 3.3mp cooled CCD camera and analysed using the IPLab Spectrum
332 software.

333 **Immunofluorescence**

334 Slides were processed as described above and blocked in 10% heat inactivated donkey
335 serum for 2 hours. Slides were incubated overnight at 4°C with α -WT1 (1:33,000) antibody
336 diluted in 1% heat inactivated donkey serum in TBSTw. Slides were incubated for 1 hour in a
337 secondary anti-rabbit AlexaFluor 488 antibody (1:800) in 1% heat inactivated donkey serum
338 and mounted in ProLong Gold mounting media containing DAPI overnight before being
339 imaged in a fluorescent stereomicroscope.

340 **Tissue staining**

341 Live bone staining was performed using 0.2% (w/v) calcein or using 50 µg/ml alizarin red as
342 previously described (Du *et al.*, 2001; Kimmel et al., 2010).

343 For cartilage and bone staining, alcian blue and alizarin red following the protocol outlined in
344 (Walker and Kimmel, 2007) with modifications from protocols on www.zfin.org.

345 **RNA Extraction and microarray analysis**

346 Fifty *Tg(wt1b:GFP)* zebrafish larvae were needle injured and grown to 72 hpi with age-
347 matched non-injured controls. The area around the site of injury was dissected (Figure 4B)
348 and transferred into 1 ml of chilled RNA-later. The samples were centrifuged into a pellet at
349 4°C and mascerated in 500 µl of Trizol® (Sigma-Aldrich) using a 25G^{5/8} 1 ml syringe. RNA
350 was extracted following Trizol® manufacturer's instructions and eluted into 15 µl of distilled
351 H₂O. Extracted RNA was sent to Myltenyi Biotec (Germany) who conducted the microarray
352 analysis. Injured and non-injured samples were sent in triplicates and the RNA was amplified
353 and Cy3-labelled using a Low Input Quick Amp Labelling Kit (Agilent Technologies) following
354 manufacturer's instructions. The labelled cRNA was hybridised against a 4x44K Whole
355 Zebrafish (V3) Genome Oligo Microarray (Agilent Technologies). The microarray images
356 were read out and processed using the Feature Extraction Software (FES – Agilent
357 Technologies) and differential gene expression was determined using the Rosetta Resolver®
358 gene expression data analysis system (Rosetta Biosoftware).

359 **Fluorescence-Activated Cell Sorting**

360 The trunk region of fifty *Tg(wt1b:GFP; R2-col2a1a:RFP)* injured larvae and non-injured 72 hpi
361 larvae were dissected and collected separately in cold PBS+2% fetal calf serum (FCS).
362 Tissue disassociation was adapted from a previously described protocol (Manoli and Driever,
363 2012) and centrifuged cells were collected in FACSmax cell disassociation solution
364 (Genlantis) . The samples were passed twice through a 40 µm cell strainer, collected in an
365 agar-coated petri dish on ice and transferred into an eppendorf tube to be sorted by a
366 FACSria2 SORP instrument (BD) equipped with a 405nm, a 488nm and a 561nm laser.
367 Green fluorescence was detected using GFP filters 525/50BP and 488nm laser, red
368 fluorescence was detected using 585/15BP filter and 561nm laser. Data was analyzed using
369 FACSDiva software (BD) Version 6.1.3.

370 **Vertebrae size measurements and statistical analysis**

371 The vertebrae size difference in injured zebrafish larvae (age range 30 dpi to 38 dpi) were
372 compared between vertebrae at the site of injury (injured) and vertebrae outside of the site of

373 injury (uninjured). Injured vertebrae and uninjured vertebrae were measured and the average
374 length was recorded for each group. The average lengths were then compared and the
375 relative size difference was calculated. The relative size difference between each group
376 (injured:uninjured vs. uninjured:uninjured) was compared using an unpaired t-test.

377

378 **Acknowledgements**

379 We thank Craig Nicol for assistance with figure design, Andrea Coates for critical reading of
380 the manuscript, and the Zebrafish Facility staff at the MRC Human Genetics Unit for zebrafish
381 husbandry.

382

383 **Competing Interests**

384 The authors have no competing interests.

385

386 **References**

387 Apschner, A., Schulte-Merker, S., and Witten, P.E. (2011) Not all bones are created equal -
388 using zebrafish and other teleost species in osteogenesis research. *Methods Cell Biol.*, 105:
389 239-55.

390

391 Asahina, K., Zhou, B., Pu, W. and Tsukamoto, H. (2011) Septum transversum-derived
392 mesothelium gives rise to hepatic stellate cells and perivascular mesenchymal cells in
393 developing mouse liver. *Hepatology*, 53(3): 983-995.

394 Bensimon-Brito, A., Cardeira, J., Cancela, M.L., Huysseune, A., Witten, P.E. (2012) Distinct
395 patterns of notochord mineralization in zebrafish coincide with the localization of Osteocalcin
396 isoform 1 during early vertebral centra formation. *BMC Dev Biol.*, 12: 28.

397 Bollig, F., Perner, B., Besenbeck, B., Kothe, S., Ebert, C., Taudien, S. and Englert, C. (2009)
398 A highly conserved retinoic acid responsive element controls wt1a expression in the zebrafish
399 pronephros. *Development*, 136(17): 2883-2892.

400

401 Carmona, R., Cano, E., Mattiotti, A., Gaztambide, J. and Muñoz-Chápuli, R. (2013) Cells
402 Derived from the Coelomic Epithelium Contribute to Multiple Gastrointestinal Tissues in
403 Mouse Embryos. *PLoS ONE*, 8(2): e55890.

404

405 Chau, Y., Bandiera, R., Serrels, A., Martínez-Estrada, O., Qing, W., Lee, M., Slight, J.,
406 Thornburn, A., Berry, R., McHaffie, S., et al. (2014) Visceral and subcutaneous fat have
407 different origins and evidence supports a mesothelial source. *Nature Cell Biology*, 16(4): 367-
408 375.

409

410 Dale, R. M. and Topczewski, J. (2011) Identification of an evolutionarily conserved regulatory
411 element of the zebrafish col2a1a gene, *Developmental biology*, 357(2): 518-531.

412

413 Deasey, S., Grichenko, O., Du, S., Nurminskaya, M. (2012) Characterization of the
414 transglutaminase gene family in zebrafish and in vivo analysis of transglutaminase-dependent
415 bone mineralization. *Amino Acids*, 42(2-3): 1065-1075.

- 416
417 Du, S. J., Frenkel, V., Kindschi, G. and Zohar, Y. (2001) Visualizing normal and defective
418 bone development in zebrafish embryos using the fluorescent chromophore calcein.
419 *Developmental biology*, 238(2): 239-246.
- 420
421 Ellis, K., Hoffman, B.D., Bagnat, M. (2013) The vacuole within: how cellular organization
dictates notochord function. *Bioarchitecture*, 3(3): 64-68.
- 422
423 Essafi, A., Webb, A., Berry, R., Slight, J., Burn, S., Spraggon, L., Velecela, V., Martinez-
424 Estrada, O., Wiltshire, J., Roberts, S. et al. (2011) A Wt1-Controlled Chromatin Switching
425 Mechanism Underpins Tissue-Specific Wnt4 Activation and Repression. *Developmental Cell*,
426 21(3), 559-574.
- 427
428 Fleming, A., Keynes, R., Tannahill, D. (2004) A central role for the notochord in vertebral
patterning. *Development*, 31(4): 873-880.
- 429
430 Gavaia, P.J., Simes, D.C., Ortiz-Delgado, J.B., Viegas, C.S., Pinto, J.P., Kelsh, R.N.,
431 Sarasquete, M.C., Cancela, M.L. (2006) Osteocalcin and matrix Gla protein in zebrafish
432 (*Danio rerio*) and Senegal sole (*Solea senegalensis*): comparative gene and protein
expression during larval development through adulthood. *Gene Expr Patterns*, 6(6): 637-652.
- 433
434 Garcia, J., Bagwell, J., Njaine, B., Norman, J., Levic, D.S., Wopat, S., Miller, S.E., Liu, X.,
435 Locasale, J.W., Stainier, D.Y.R., Bagnat, M. (2017) Sheath Cell Invasion and Trans-
436 differentiation Repair Mechanical Damage Caused by Loss of Caveolae in the Zebrafish
Notochord. *Current Biology*, 27(13): 1982-1989.
- 437
438 Hastie, N.D. (2017) Wilms' tumour 1 (WT1) in development, homeostasis and disease.
439 *Development* (in press).
- 440
441 Huitema, L. F., Apschner, A., Logister, I., Spoorendonk, K. M., Bussmann, J., Hammond, C.
442 L. and Schulte-Merker, S. (2012) *Entpd5* is essential for skeletal mineralization and regulates
443 phosphate homeostasis in zebrafish. *Proceedings of the National Academy of Sciences of the*
444 *United States of America*, 109(52): 21372-21377.
- 445
446 Kawakami, K. (2007) Tol2: a versatile gene transfer vector in vertebrates. *Genome biology*, 8
447 Suppl 1: S7.
- 448
449 Kimmel, C. B., DeLaurier, A., Ullmann, B., Dowd, J. and McFadden, M. (2010) Modes of
450 developmental outgrowth and shaping of a craniofacial bone in zebrafish. *PloS one*, 5(3):
451 e9475.
- 452
453 Kreidberg, J., Sariola, H., Loring, J., Maeda, M., Pelletier, J., Housman, D., and Jaenisch, R.
454 (1993). WT-1 is required for early kidney development. *Cell*, 74(4): 679-691.
- 455
456 Lawson, L. and Harfe, B.D. (2015) Notochord to Nucleus Pulposus Transition. *Curr*
Osteoporos Rep., 13(5):336-41.
- 457
458 Lefebvre, V. and Bhattaram, P. (2010) Vertebrate skeletogenesis. *Curr Top Dev Biol.*, 90:
291-317.
- 459
460 Manoli, M. and Driever, W. (2012) Fluorescence-activated cell sorting (FACS) of fluorescently
461 tagged cells from zebrafish larvae for RNA isolation. *Cold Spring Harbor protocols*, 8.
- 462
463 Martínez-Estrada, O., Lettice, L., Essafi, A., Guadix, J.A., Slight, J., Hall, E., Velecela, V.,
464 Reichmann, J., Devenney, P.S., Hohenstein, P. et al. (2010). Wt1 is required for
465 mesenchymal cardiovascular progenitor cell formation in epicardium and ES cells through
466 direct transcriptional control of snail 1 and E-cadherin. *Nat.Genet.*, 42(1): 89-93: e20023660.

- 467 Motamedi, F., Badro, D., Clarkson, M., Rita Lecca, M., Bradford, S., Buske, F., Saar, K.,
468 Hübner, N., Brändli, A. and Schedl, A. (2014). WT1 controls antagonistic FGF and BMP-
469 pSMAD pathways in early renal progenitors. *Nature Communications*, 5.
470
- 471 Perner, B., Englert, C. and Bollig, F. (2007) The Wilms tumor genes *wt1a* and *wt1b* control
472 different steps during formation of the zebrafish pronephros. *Developmental biology*, 309(1):
473 87-96.
474
- 475 Schnabel, K., Wu, C, Kurth, T and Weidinger, G. (2011) Regeneration of Cryoinjury Induced
476 Necrotic Heart Lesions in Zebrafish Is Associated with Epicardial Activation and
477 Cardiomyocyte Proliferation. *PLoS One*, 6(4): e18503
478
- 479 Schurgers, L.J., Uitto, J. and Reutelingsperger, C.P. (2013) Vitamin K-dependent
480 carboxylation of matrix Gla-protein: a crucial switch to control ectopic mineralization. *Trends*
481 *Mol Med.*, 19(4): 217-226.
482
- 483 Smart, N., Bollini, S., Dube, K. N., Vieira, J. M., Zhou, B., Davidson, S., Yellon, D., Riegler, J.,
484 Price, A. N., Lythgoe, M. F. et al. (2011) De novo cardiomyocytes from within the activated
485 adult heart after injury. *Nature*, 474: 640-644.
- 486 Stemple DL. (2005) Structure and function of the notochord: an essential organ for chordate
487 development. *Development*, 132(11): 2503-2512
- 488 Sweatt, A., Sane, D.C., Hutson, S.M., Wallin, R. (2003) Matrix Gla protein (MGP) and bone
489 morphogenetic protein-2 in aortic calcified lesions of aging rats. *J Thromb Haemost.*, 1(1):
490 178-185.
491
- 492 Walker, M. B. and Kimmel, C. B. (2007) 'A two-color acid-free cartilage and bone stain for
493 zebrafish larvae', *Biotechnic & histochemistry: official publication of the Biological Stain*
494 *Commission*, 82(1): 23-28.
495
- 496 White, R. M., Sessa, A., Burke, C., Bowman, T., LeBlanc, J., Ceol, C., Bourque, C., Dovey,
497 M., Goessling, W., Burns, C. E. et al. (2008) Transparent adult zebrafish as a tool for in vivo
498 transplantation analysis. *Cell stem cell*, 2(2): 183-189.
499
- 500 Wojciechowska, S., Zeng, Z., Lister, J. A., Ceol, C. J. and Patton, E. E. (2016) Melanoma
501 Regression and Recurrence in Zebrafish. *Methods in molecular biology*, 1451: 143-53.
502
- 503 Yamamoto, M., Morita, R., Mizoguchi, T., Matsuo, H., Isoda, M., Ishitani, T., Chitnis, A. B.,
504 Matsumoto, K., Crump, J. G., Hozumi, K. et al. (2010) Mib-Jag1-Notch signalling regulates
505 patterning and structural roles of the notochord by controlling cell-fate decisions.
506 *Development*, 137(15): 2527-2537.
507
- 508 Zebboudj, A.F., Imura, M., Boström, K. (2002) Matrix GLA protein, a regulatory protein for
509 bone morphogenetic protein-2. *J Biol Chem*, 277(6): 4388-4394.
510

511 **Video 1 Legend**

512 Time-lapse imaging of two-photon microscopy of *Tg (wt1b:GFP; col2a1a:RFP)* zebrafish
513 larvae following needle injury over 48 hours. *wt1b:GFP* expression is upregulated
514 in *col2a1a:RFP* expressing notochord sheath cells upon needle injury, leading to the
515 formation of a stopper like structure across the wound

516
517
518
519
520
521
522
523
524

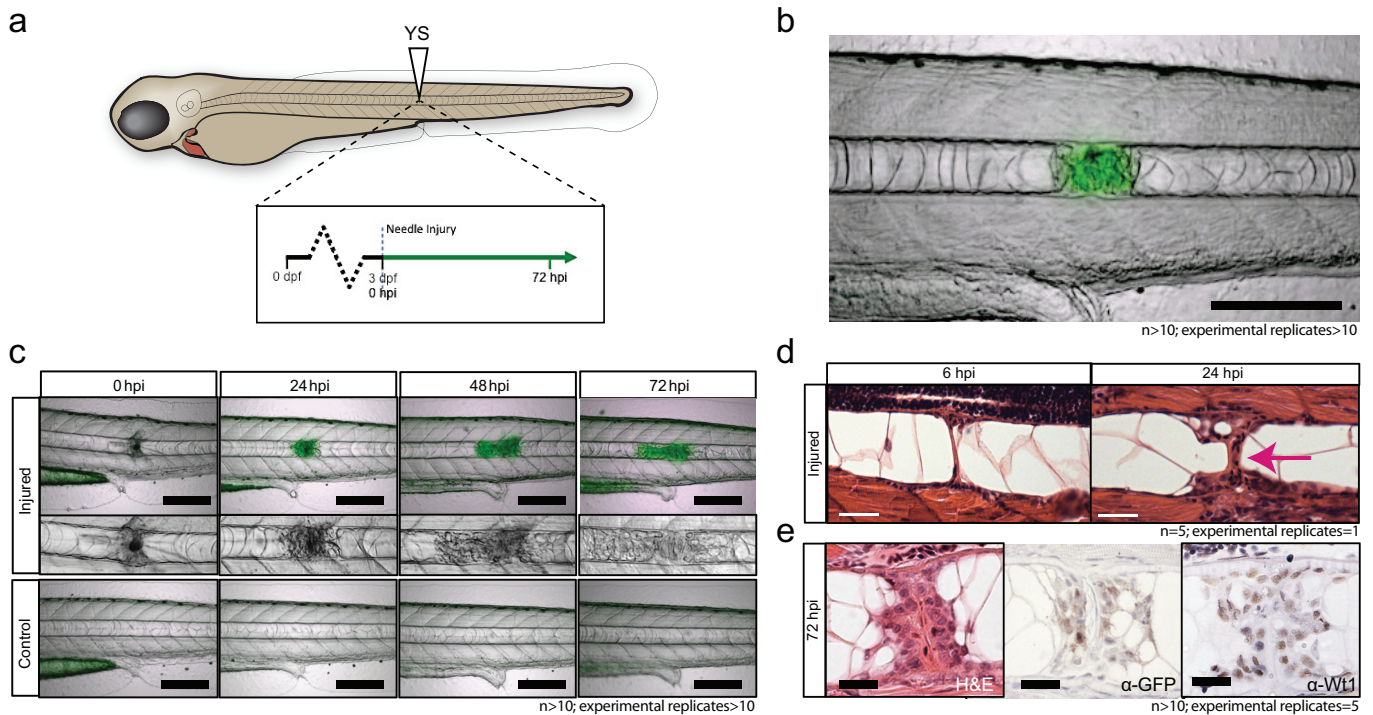


Figure 1. Notochord injury triggers a local and sustained expression Wt1.

(a) Schematic of notochord needle-injury protocol. 3 dpf *Tg(wt1b:GFP; casper)* larvae are injured above the yolk sac (YS) and followed for 72 hours.

(b, c) Images of *Tg(wt1b:GFP; casper)* zebrafish trunk over time following notochord needle injury, and uninjured matched controls. GFP signal is associated with a change of cellularity in the injured notochord (inset). n>10; experimental replicates>10. Scale bar: 100 μ m.

(d) H&E staining of the injured area at 6 hpi and 24 hpi highlighted the progressive change in cellularity at the site of the injury (arrow). n=5; experimental replicates=1. Scale bar: 20 μ m.

(e) Immunohistochemistry of the injured area with α -GFP and α -Wt1 antibodies. n>10; experimental replicates=5. Scale bar: 20 μ m.

dpf = days post fertilization; hpi = hours post injury; H&E= haematoxylin and eosin.

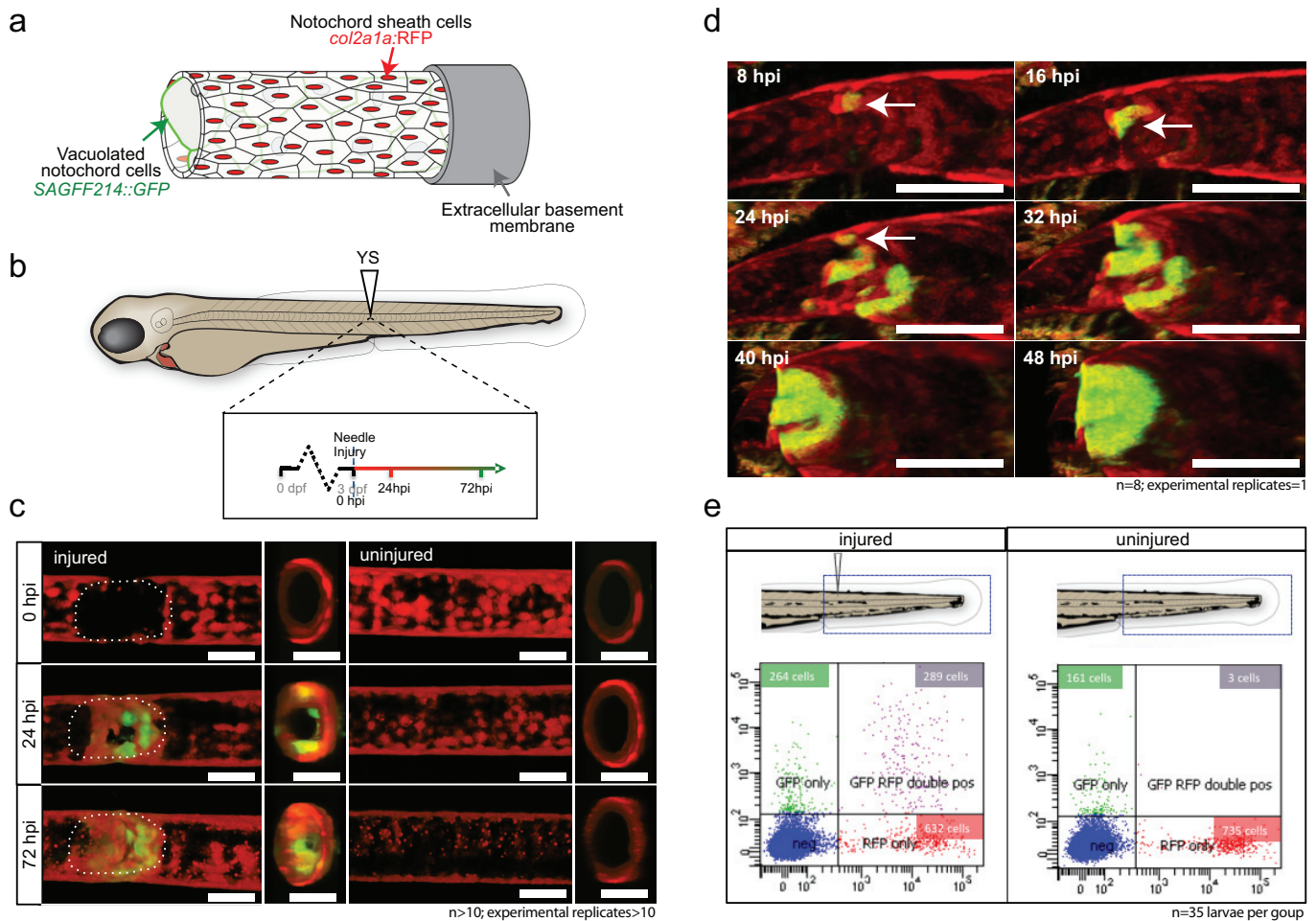


Figure 2. *wt1b:GFP* expressing notochord sheath cells populate the site of injury in the damaged notochords.

(a) Schematic diagram of the notochord and transgenic lines used in this study. The notochord is composed of an inner population of highly vacuolated cells (green arrow), surrounded by a layer of epithelial-like sheath cells (red arrow), encapsulated by a thick layer of extracellular basement membrane (grey arrow).

(b) Schematic of experimental design: 3 dpf *Tg(wt1b:GFP; col2a1a:RFP; casper)* larvae were needle-injured and imaged at 0, 24 and 72 hpi.

(c) Needle damage led to the formation of a cell-less gap in the layer of notochord sheath cells (0 hpi – injured; dashed line). GFP expression can be observed in the notochord sheath cells surrounding the area of damage by 24 hpi (inset) and these appear to engulf the injured area by 72 hpi (inset). n > 10; experimental replicates > 10. Scale bar: 100 μ m.

(d) Multiphoton time-lapse imaging of wound site. Initial upregulation of GFP occurs at 8 hpi in the *col2a1a:RFP* positive cells (arrow) and propagates across the injured area over the next 40 hours. n = 8; experimental replicates = 1. Scale bar: 100 μ m.

(e) FACS analysis of cell populations in injured and non-injured zebrafish trunk tissue. GFP+RFP+ double positive cells are present in injured *Tg(wt1b:GFP; col2a1a:RFP)* at 72 hpi (n=35 larvae per group).

dpf = days post fertilization; hpi = hours post injury.

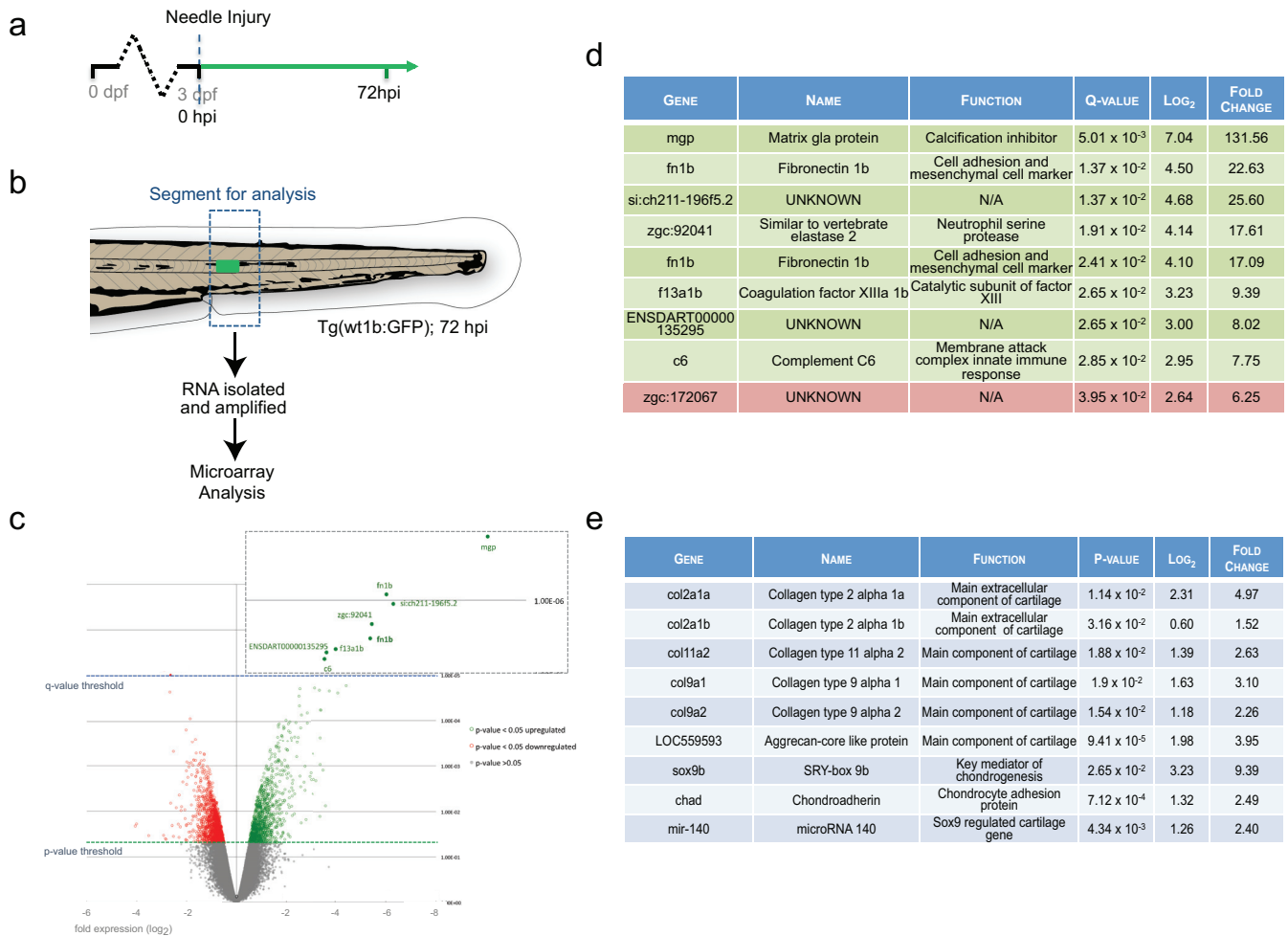


Figure 3. Cartilage genes are expressed in the notochord-injured zebrafish.

(a) Experimental plan: 3 dpf *Tg(wt1b:GFP)* larvae were needle injured and grown for 72 hours with uninjured age-matched controls (n = 50 larvae per group).

(b) Schematic of the area around the *wt1b:GFP* expression was excised at 72 hpi (dotted area) and RNA was extracted and amplified. A similar area was taken from age-matched uninjured controls.

(c) Volcano plot displaying the differentially expressed genes between injured and non-injured larvae. The y-axis measures the mean expression value of log₁₀ (p-value) and separates upregulated from downregulated genes. The x-axis represents the log₂ fold change of expression. Significantly upregulated genes are shown as green circles or dots and downregulated genes are shown as red circles or dots. Green dotted line represents the p-value threshold (p < 0.05) and blue dotted line represents the false discovery rate (FDR) or q-value threshold (q < 0.05). Genes with highest expression change in magnified view.

(d) Table showing the most significantly differentially expressed genes in injured larvae (q < 0.05). Upregulated genes are shown in green and downregulated genes are shown in red.

(e) Table showing cartilage-associated genes that were significantly upregulated in the injured larvae (p < 0.05).

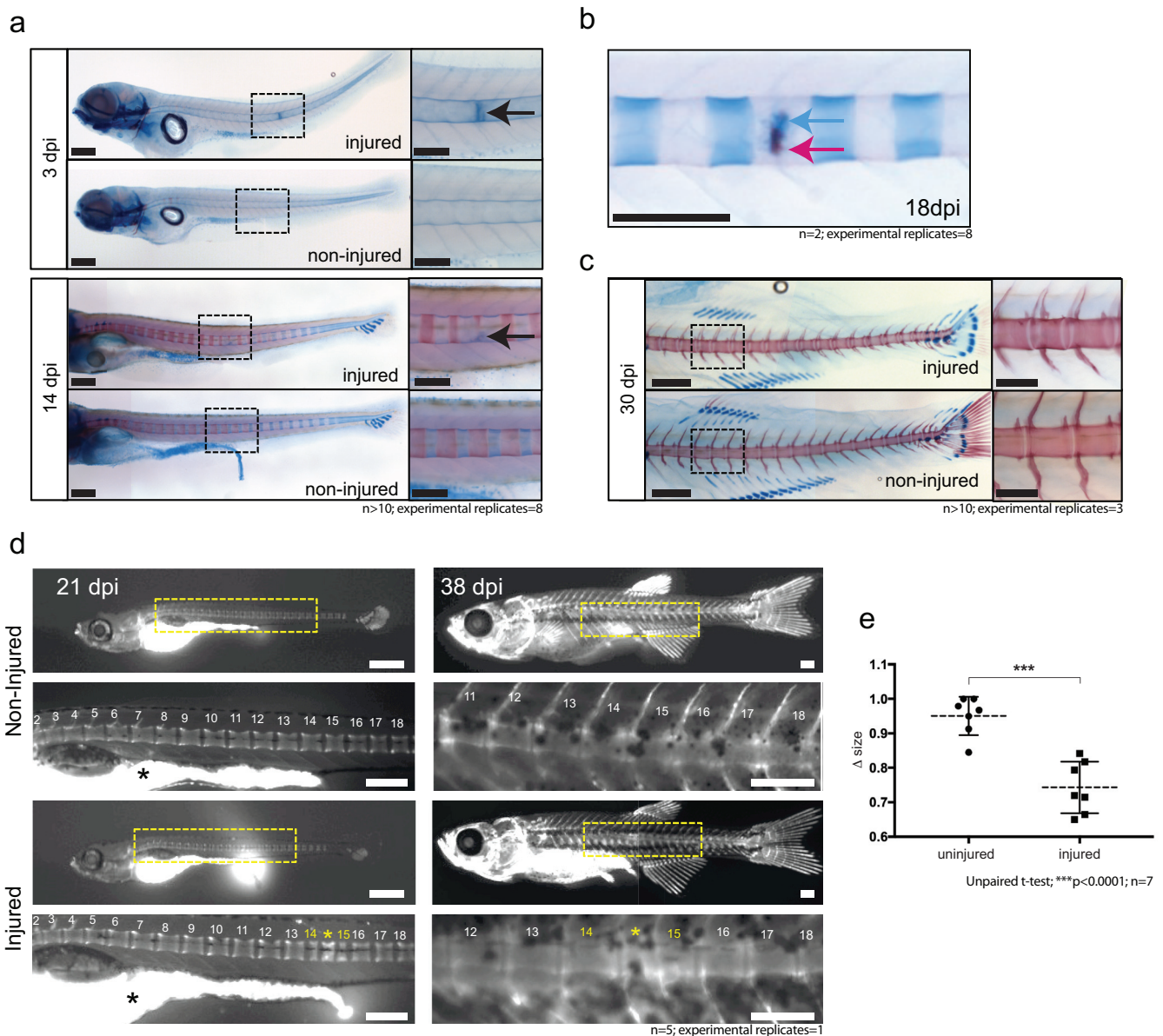


Figure 4. Ectopic vertebra formation occurs via a cartilage intermediate at the site of injury.

(a) Alcian blue staining (cartilage staining) at the site of injury in 3 and 14 dpi larvae. Ectopic cartilage deposit is indicated by arrow. n >10; experimental replicates = 8. Scale bar left panels: 400μm; scale bar right panels (zoomed images): 200μm.

(b) Alcian blue and alizarin red (bone) staining at the site of injury 18 dpi indicates the presence of bone and cartilage at the repair site (blue arrow = cartilage; red arrow = bone). n = 2; experimental replicates = 8. Scale bar: 200μm.

(c) Alcian blue and alizarin red staining of 30 dpi larvae reveals the formation of a smaller vertebra/vertebrae around the area of damage in injured larvae. n >10; experimental replicates = 3. Scale bar left panels: 400μm; scale bar right panels (zoomed images): 200μm.

(d) Live imaging of calcein stained zebrafish at 21 and 38 dpi in injured and uninjured fish. Extra vertebrae are indicated by (yellow asterisk). Black asterisk denotes intestinal fluorescence. n =5; experimental replicates = 1. Scale bar 21 hpf: 200μm; scale bar 21 hpf zoomed: 100μm; scale bar 38 hpf: 200μm; scale bar 38 hpf zoomed: 100μm.

(e) The relative vertebra size difference (Δ size) between vertebrae at the site of injury (injured) and vertebrae in non-injured areas (uninjured). Vertebrae at the site of injury were significantly smaller than uninjured vertebrae (Unpaired t-test; *** p < 0.0001 two-tailed; mean +/- SEM uninjured larvae =0.9506 +/- 0.02102 n = 7; mean +/- SEM injured larvae =0.7432 +/- 0.0284 n = 7; measurements taken at 30 and 38 dpi).

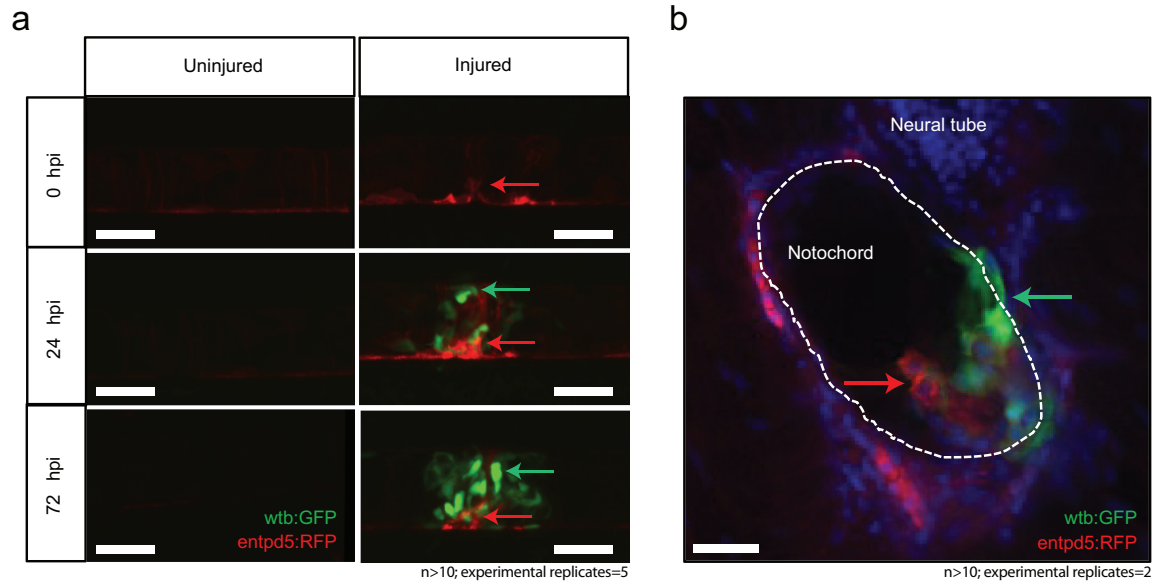


Figure 5. Distinct and closely associated *wt1* and *entpd5* subpopulations emerge at the damage site.

(a) Live-imaging at the site of notochord injury in *Tg(wt1b:GFP; entpd5:RFP)* larvae. Expression of *wt1b:GFP* and *entpd5:RFP* at site of damage (green arrows and red arrows respectively) in injured and uninjured fish. n >10; experimental replicates = 5. Scale bar: 50 μ m.

(b) Cryo-section of the injured area confirms distinct *wt1b:GFP* and *entpd5:RFP* subpopulations at site of damage. n >10; experimental replicates = 2. Scale bar: 20 μ m.

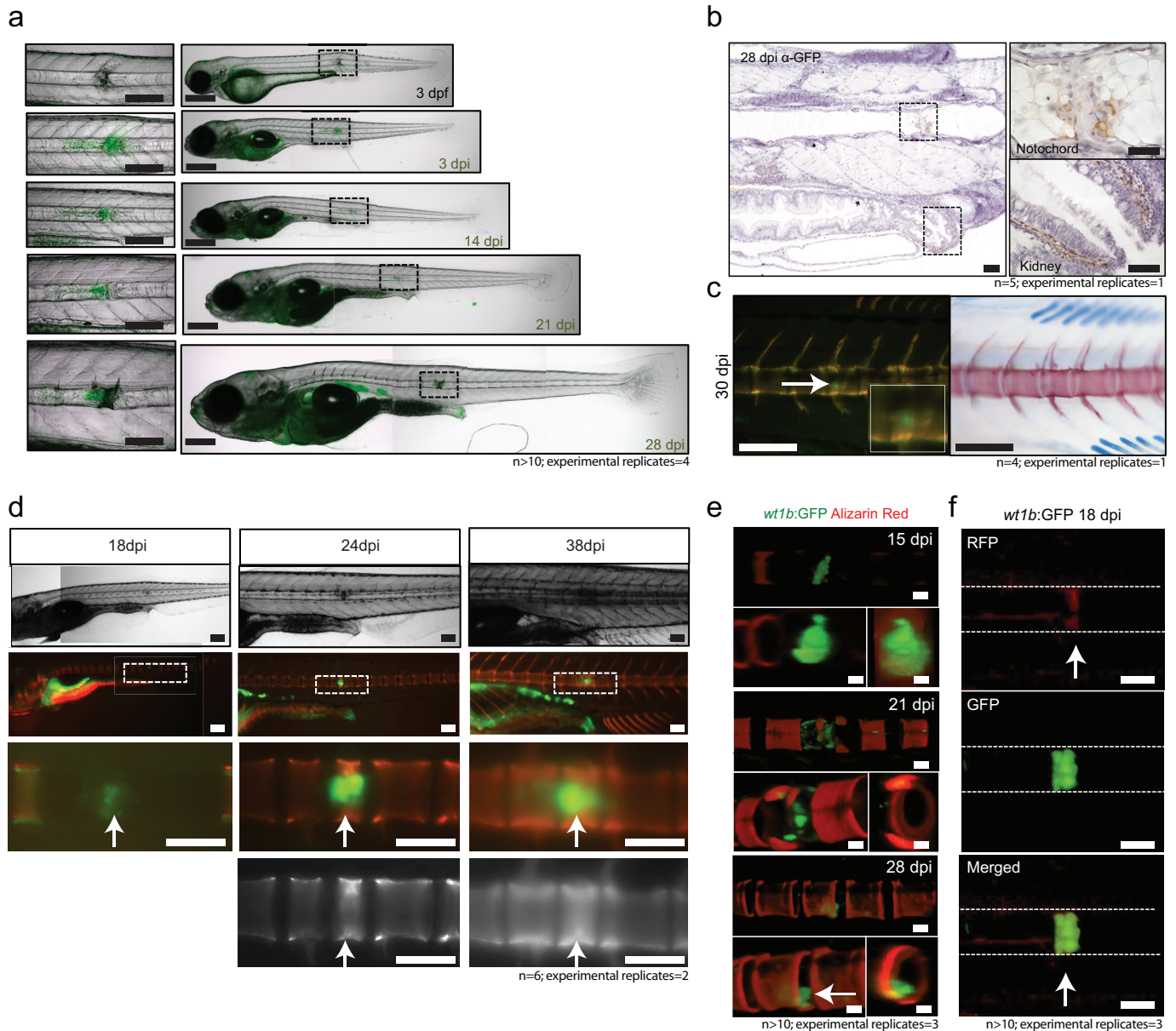


Figure 6. *wt1b* expressing cells are closely associated with vertebral development after injury.

(a) Images of *wt1b:GFP* zebrafish following needle injury at 3dpf and raised to 28 dpi. n >10; experimental replicates = 4. Scale bar left panels: 100 μ m; scale bar right panels: 200 μ m.

(b) α -GFP staining of 28 dpi larvae at the site of the healing notochord wound and in the kidney. n = 5; experimental replicates = 1. Scale bar left panels: 50 μ m.

(c) Image of fish from Figure 5A, stained with alizarin red and imaged for *wt1b:GFP* expressing cells. GFP positive cells are found within the ectopic vertebra (white arrow and inset). n = 4; experimental replicates = 1. Scale bar left panels: 100 μ m.

(d) Long term follow up of alizarin red stained Tg(*wt1b:GFP*; *casper*) larvae shows that chordacentra formation is delayed around the site of injury. GFP cells mark the site of the future ectopic vertebra. n = 6; experimental replicates = 2. Scale bar: 100 μ m; scale bar zoomed images: 50 μ m

(e) Confocal imaging of 15, 21 and 28 dpi larvae reveals an overlapping expression between the *wt1b:GFP* expressing cells and the forming chordacentra (alizarin red stained) in the injured Tg(*wt1b:GFP*; *casper*) larvae. n >10; experimental replicates = 3. Scale bar: 100 μ m.

(f) Confocal imaging highlights the overlapping presence of bone (alizarin red stained) and *wt1b:GFP* cells at the wound in 18 dpi larvae (arrow). n >10; experimental replicates = 3. Scale bar: 100 μ m.

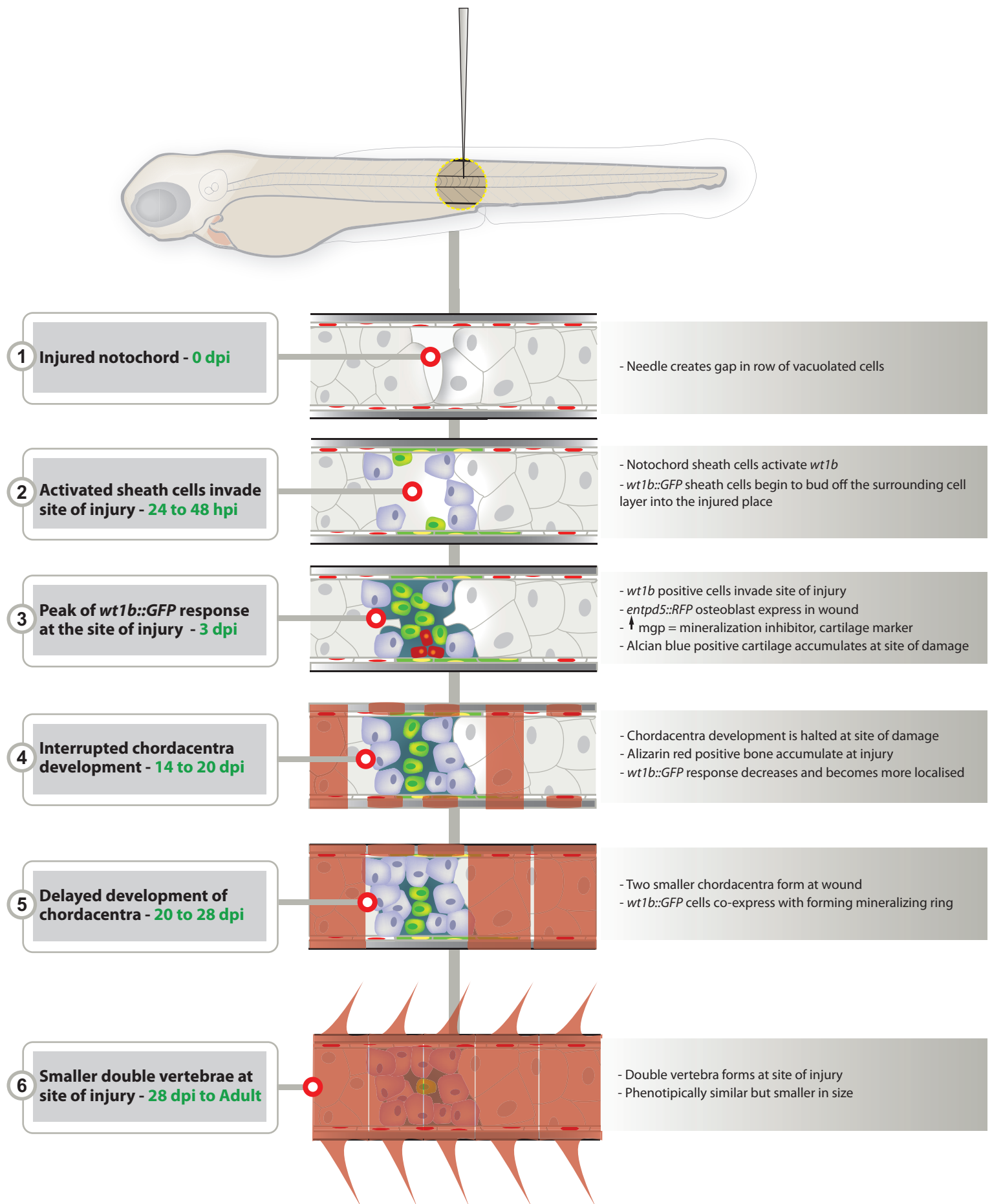


Figure 7. Schematic of the notochord wound response.